European Radiology (2019) 29:2989–2997
https://doi.org/10.1007/s00330-018-5756-9

CHEST

Identification of epidermal growth factor receptor mutations in pulmonary adenocarcinoma using dual-energy spectral computed tomography

Meng Li[1] · Li Zhang[1] · Wei Tang[1] · Yu-Jing Jin[1] · Lin-Lin Qi[1] · Ning Wu[1,2]

Received: 10 May 2018 / Revised: 25 July 2018 / Accepted: 12 September 2018 / Published online: 26 October 2018

Abstract

Objectives To explore the role of dual-energy spectral computed tomography (DESCT) quantitative characteristics for the identification of epidermal growth factor receptor (EGFR) mutation status in a cohort of East Asian patients with pulmonary adenocarcinoma.

Materials and methods Patients with lung adenocarcinoma who underwent both DESCT chest examination and EGFR test were retrospectively selected from our institution's database. The DESCT visual morphological features and quantitative parameters, including the CT number at 70 keV, normalized iodine concentration (NIC), normalized water concentration, and slopes of the spectral attenuation curves (slope λ HU [Hounsfield unit]), were evaluated or calculated. The patients were divided into two groups: the EGFR mutation group and EGFR wild-type group. Statistical analyses were performed to identify the DESCT quantitative parameters for diagnosis of EGFR mutation status.

Results EGFR mutations were detected in 66 (55.0%) of the 120 enrolled patients. The univariate analysis revealed that sex, smoking history, CT texture, NIC, and slope λ HU were significantly associated with EGFR mutation status (p = 0.037, 0.001, 0.047, 0.010, and 0.018, respectively). The multivariate logistic analysis revealed that smoking history (odds ratio [OR] = 3.23, p = 0.005) and NIC (OR = 58.026, p = 0.049) were the two significant predictive factors associated with EGFR mutations. Based on this analysis, the smoking history and NIC were combined to determine the predictive value for EGFR mutations with the area under the curve of 0.702.

Conclusions NIC may be a potential quantitative DESCT parameter for predicting EGFR mutations in patients with pulmonary adenocarcinoma.

Key Points

- *DESCT can provide multiple quantitative image parameters compared to conventional CT.*
- *Identification of the radio-genomic relation between DESCT and EGFR status can help to define molecular subcategories of lung adenocarcinoma, which is valuable for personalized clinical targeted therapy.*
- *NIC may be a potential DESCT quantitative parameter for predicting EGFR mutations in pulmonary adenocarcinoma.*

Keywords Tomography, X-ray computed · Epidermal growth factor receptor · Lung neoplasms · Adenocarcinoma

✉ Ning Wu
cjr.wuning@vip.163.com

[1] Department of Diagnostic Radiology, National Cancer Center/National Clinical Research Center for Cancer/Cancer Hospital, Chinese Academy of Medical Sciences and Peking Union Medical College, Beijing, China

[2] PET-CT Center, National Cancer Center/National Clinical Research Center for Cancer/Cancer Hospital, Chinese Academy of Medical Sciences and Peking Union Medical College, Beijing, China

Abbreviations

ALK	Anaplastic lymphoma kinase
DESCT	Dual-energy spectral computed tomography
EGFR	Epidermal growth factor receptor
GGO	Ground-glass opacity
GSI	Gemstone spectral imaging
KRAS	Kirsten rat sarcoma viral oncogene homolog
NIC	Normalized iodine concentration

NWC	Normalized water concentration
PSN	Part-solid nodule
Slope λ HU	The slope of the spectral Hounsfield unit curve
SSN	Sub-solid nodule

Introduction

Pulmonary adenocarcinoma is the most common histologic form of lung cancer and has been considered a highly heterogeneous disease based on its molecular biological features [1–3]. There are three most common mutations: epidermal growth factor receptor (EGFR), anaplastic lymphoma kinase (ALK), and Kirsten rat sarcoma viral oncogene homolog (KRAS). Among the three, EGFR is the most important and well-studied oncogene as a therapeutic target. Compared to patients treated with standard chemotherapy, patients treated with EGFR tyrosine kinase inhibitors have exhibited better response rates and prolonged progression-free survival [4, 5].

EGFR mutations have been found to correlate with specific clinical characteristics, such as the female sex, smoking status, and East Asian ethnicity [6, 7]. Some radio-genomic research has attempted to correlate computed tomography (CT) features with EGFR mutations to classify subcategories of lung adenocarcinoma. Most of these studies have focused on ground-glass opacity (GGO) nodules and demonstrated that the GGO ratio was significantly higher in tumors with EGFR mutations than that in EGFR wild-type tumors [8–13]. Additionally, other CT features, such as pleural indentation and the vacuole sign, may also be associated with EGFR mutations [9]. However, these CT features are vulnerable to subjective judgment that cannot be used as a quantitative evaluation.

Dual-energy spectral computed tomographic (DESCT) is a new revolutionary CT imaging method, which can improve material differentiation by using two different X-ray energy spectra [14, 15]. DESCT with gemstone spectral imaging (GSI) scan uses a fast and dynamic kVp switching technique between 80 and 140 kVp during one single rotation, which can generate 101 monochromatic CT images at energy levels from 40 to 140 keV, iodine-based and water-based material decomposition images, etc. Therefore, some quantitative measurements can be obtained from DESCT, such as monochromatic CT number and the slope of the spectral Hounsfield unit (HU) curve (slope λ HU), iodine concentration (IC), and water concentration (WC) from material decomposition images. It has been proven that DESCT has potential applications in various clinical areas, including diagnosis in oncology [14, 16, 17]. Especially for lung cancer, DESCT has been employed to differentiate cancers from benign lung nodules, to identify lymph node metastases, and to distinguish the histologic subtypes such as adenocarcinoma and squamous cell carcinoma [18–25].

Therefore, exploring the relationship between DESCT quantitative measurements and EGFR status may help determine the molecular categories of lung adenocarcinoma. To the best of our knowledge, there are no previous reports in the literature regarding the application of DESCT for the preoperative diagnosis of EGFR status in patients with lung adenocarcinoma. Thus, the purpose of this study was to retrospectively investigate the feasibility of using quantitative measurements of DESCT parameters to identify EGFR mutation status in a cohort of Chinese patients with lung adenocarcinomas.

Materials and methods

Patient selection

The study cohort was retrospectively selected from a prospectively collected and recorded database of patients with lung nodules and masses that were scheduled to undergo pretreatment chest DESCT between May 2013 and December 2015 at our institution. The inclusion criteria consisted of a histopathological diagnosis of adenocarcinoma and EGFR mutations test at our institution (Fig. 1). All histological and mutation analyses were performed for surgical specimens (obtained during radical surgery or palliative surgery) or biopsy specimens. Finally, a total of 120 patients with lung adenocarcinoma (54 males and 66 females; age range, 28–78 years; median age, 58 years) were included in this study.

This study was approved by the Institutional Review Board at the Cancer Hospital of the Chinese Academy of Medical Sciences. Since the study was retrospective and the data were analyzed anonymously, the need for written informed consent was waived.

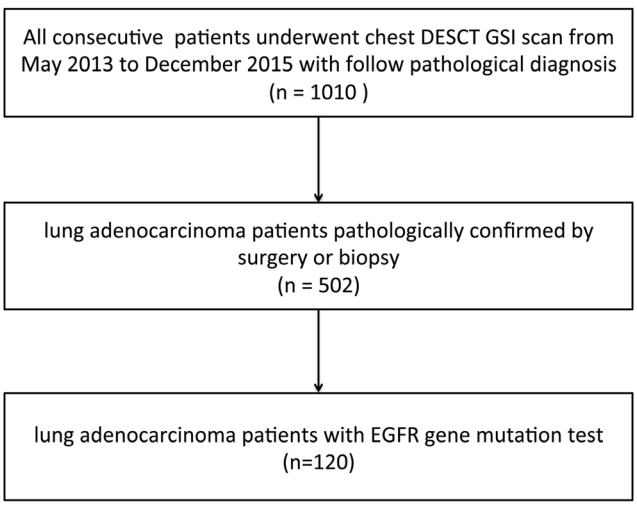

Fig. 1 Flowchart depicting the patient selection

CT examination and post-processing

All DESCT examinations were performed using a Discovery CT 750 HD scanner (GE Healthcare) before treatment. The scanning parameters were as follows: fast switching tube voltage between 80 and 140 kVp, with a cycle of 0.5 ms; tube current of 550 mA; tube rotation time of 0.6 s; helical mode, pitch of 0.984; collimation of 40 mm; large body field-of-view (FOV); slice thickness/interval for axial images, 1.25 mm/0.8 mm; and scan coverage from the apex of the lung to the adrenal gland. All patients were intravenously injected with 85–95 ml of contrast media (300 mg/ml) using a power injector at a rate of 2.5 ml/s. Scan acquisition commenced after a 35-s delay.

The original data acquired from DESCT were reconstructed into material decomposition images and monochromatic images. The reconstructed images were sent to a post-processing workstation (Advantage Workstation 4.6, GE Healthcare). Gemstone Spectral Imaging (GSI) Volume Viewer software (GE Healthcare) was used to acquire and analyze the DESCT quantitative parameters on the workstation.

DESCT image analysis

The visual analyses of morphological features were conducted by two experienced radiologists. The morphological CT texture features included solid nodule (SN), part-solid nodule (PSN) or mixed GGO, and non-solid nodule (NSN) or pure GGO; NSN was defined as a hazy increased opacity of lung, with preservation of bronchial and vascular margins; PSN was defined as a combination of ground glass and solid attenuation, which obscures the underlying lung architecture on CT; the NSN and PSN were both referred to as sub-solid nodule (SSN) [26–29]. Other morphological features including tumor size (the longest diameter on the transverse lung window image), lobulation, spiculation, air bronchogram, vacuole sign, and pleural retraction were also evaluated.

For quantitative analysis, the thoracic CT images were evaluated by a radiologist with 10 years of experience interpreting thoracic CT images. Regions of interest (ROI) were placed at the center of the tumor that was selected on the axial CT slice to depict its maximum diameter manually. For SN, the tumors were measured in a mediastinum window (wide = 350, level = 50). For SSN, the ROIs were measured in a lung window (wide = 1500, level = -600), within which the entire tumor could be visualized.

The IC and WC of each lesion were measured from the iodine- and water-based material decomposition images. To minimize the variations caused by the patient's circulation status and the scanning times, the IC and WC of each lung lesion were normalized to the IC and WC of the thoracic aorta, respectively, where IC was normalized as $NIC = IC_{lesion}/IC_{aorta}$ and WC was normalized as $NWC = WC_{lesion}/WC_{aorta}$ at the T6 level. The GSI software automatically propagated the ROIs to all monochromatic images with energies from 40 to 140 keV to generate the spectral attenuation curves. The slope λ HU was calculated as slope $\lambda\ HU = (CT_{40\ keV} - CT_{100\ keV})/(100–40)$. The enhanced CT numbers on the 70 keV monochromatic images (CT number at 70 keV) were also measured because the conventional polychromatic images at 120 kVp had an average energy of approximately 70 keV in GSI mode. To summarize, four types of quantitative data were obtained from the DESCT images: the CT number at 70 keV, NIC, NWC, and slope λ HU.

EGFR mutation analysis

A molecular analysis of the mutation status of the EGFR was examined with a polymerase chain reaction-based amplification refractory mutation system using the Human EGFR Gene Mutations Detection Kit (Beijing ACCB Biotech Ltd.). Based on the outcome of the EGFR test, the patients were divided into two groups: the EGFR mutation group and the EGFR wild-type group.

Statistical analysis

The statistical analyses were performed using the SPSS software, version 20. Quantitative data with a normal distribution were presented as means ± standard deviations. The potential factors of EGFR identification were analyzed by univariate and multivariate analyses. In univariate analyses, continuous data were compared using independent sample *t* test for normal distribution or using non-parametric K-S test for abnormal distribution; categorical data were compared using a chi-square (χ^2) test. Multiple analyses were performed to identify independent factors in order to predict EGFR mutation status. The significant factors in univariate analysis were identified as candidate covariates in a logistic regression model with backward elimination method. A receiver operating characteristic (ROC) curve was generated to estimate the predictive value of the significant factors for EGFR identification. The predictive capability was determined by calculating the area under the curve (AUC). The level of significance was defined as $p = 0.05$.

Results

Patient characteristics and EGFR mutations

The patients' characteristics are reported in Table 1. According to the outcomes of EGFR testing, 66 patients had EGFR mutations (the EGFR mutation group) and 54 patients

Table 1 Association between patients characteristics with EGFR mutation status

Variables	Total	EGFR		*p*
		+	–	
No. of patients	120	66	54	
Age (years)	55.97 ± 11.57	56.89 ± 10.76	54.85 ± 12.50	0.336
Sex				
Female	66	42	24	*0.037*
Male	54	24	30	
Smoking				
Never smoked	79	52	27	*0.001*
Smoker	41	14	27	
Location				
Peripheral	115	63	52	0.819
Central	5	3	2	
Pathology acquisition				
Radical surgery	106	60	46	
Palliative surgery	10	4	6	0.589
Biopsy	4	2	2	
TNM stage*				
I	56	33	23	
II	22	11	11	0.772
III	28	16	12	
IV	0	0	0	

Values are mean ± standard deviation or number. Significant *p* values are in italics. $P < 0.05$ indicates significant difference

*106 patients who underwent radical surgery have pathological TNM stage

exhibited no EGFR mutations (the EGFR wild-type group). The EGFR mutation rate was 55.0% (66/120).

Analysis of DESCT morphological features and quantitative parameters for EGFR mutations

The univariate analysis data for the radiographic features of EGFR mutations and wild-type disease are presented in Table 2. For morphological features, only the CT texture feature difference has statistical significant ($p = 0.047$). For DESCT quantitative parameters, the NIC and slope λ HU values differed significantly between the EGFR mutation and wild-type groups ($p = 0.010$ and $p = 0.015$, respectively; Figs. 2 and 3). However, there was no significant difference observed in CT number at 70 keV and the NWC between two groups ($p = 0.930$ and $p = 0.838$, respectively).

Moreover, multivariate logistic analysis of DESCT candidate covariates (CT texture type, NIC and slope λ HU) indicated that the NIC was the only significant DESCT quantitative parameter associated with EGFR mutations (odds ratio [OR] = 135.251, $p = 0.014$) (Table 2), and the AUC for the prediction of EGFR mutation was 0.650 (95% confidence interval [CI] 0.551–0.750, $p < 0.005$; Fig. 4). The optimal cutoff value was 0.15 with a sensitivity of 0.71 and specificity of 0.57.

Multivariate analyses of DESCT quantitative parameters and clinical features for EGFR mutations

Results from multivariate logistic analysis of DESCT and clinical candidate covariates (sex, smoking status, CT texture type, NIC, and slope λ HU) indicated that smoking history (OR = 3.23, $p = 0.005$) and NIC (OR = 58.026, $p = 0.049$) were the two significant factors associated with EGFR mutations. Based on this analysis, the two significant factors (smoking history and NIC) were combined to determine the predictive value for EGFR mutations with the AUC value of 0.702 (95% CI 0.607–0.798, $p = 0.000$; Fig. 4).

Discussion

The present study showed a significant correlation between EGFR mutations of pulmonary adenocarcinoma and NIC, a DESCT quantitative parameter, in both univariate and multivariate analyses. The pairwise comparisons demonstrated that the NIC values of the EGFR mutation group were

Table 2 Univariate and multivariate analysis of DESCT characteristics with EGFR mutation status

Variables	Total	EGFR		*p* value	Multivariate analysis*	
		+	–		OR	*p* value
Maximum tumor size	3.05 ± 1.62	2.97 ± 1.39	3.07 ± 1.88	0.728		
CT texture feature						
SN	95	48	47		Reference	
PSN (mixed GGO)	14	12	2	*0.047*	1.064	0.394
NSN (pure GGO)	11	6	5		4.010	
Other morphologic features						
Lobulation	84	46	38	0.936		
Spiculation	48	27	21	0.822		
Air bronchogram	39	25	14	0.164		
Vacuole sign	22	14	8	0.638		
Pleural retraction	61	38	23	0.102		
Quantitative parameters						
CT number at 70 keV	-7.83 ± 144.95	-6.76 ± 145.86	-9.12 ± 145.18	0.930		
NIC	0.20 ± 0.11	0.23 ± 0.12	0.17 ± 0.10	*0.010*	135.251	*0.014*
NWC	0.93 ± 0.15	0.93 ± 0.15	0.94 ± 0.15	0.838		
Slope λ HU	1.88 ± 0.97	2.07 ± 0.98	1.64 ± 0.91	*0.018*	1.652	0.959

Values are mean ± standard deviation or number. Significant *p* values are in italics. $P < 0.05$ indicates significant difference

SN solid nodule, *NSN* non-solid nodule, *PSN* part-solid nodule, *GGO* ground-glass opacity, *NIC* normalized iodine concentration, *NWC* normalized water concentration. *Slope λ HU* the slope of the spectral HU (Hounsfield unit)

*Obtained by logistic regression model with backward stepwise selection of variables

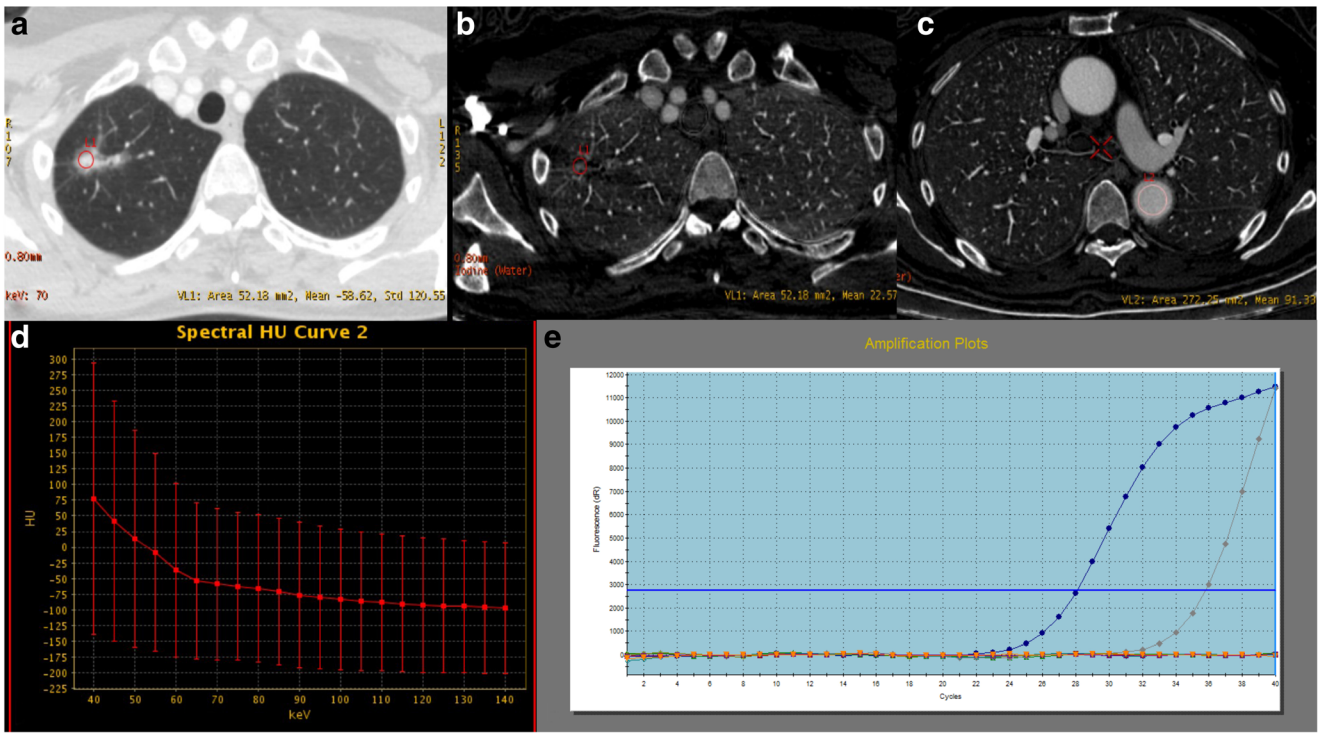

Fig. 2 Images of a 70-year-old female patient with no smoking history, diagnosed with pulmonary adenocarcinoma. **a** A dual-energy spectral computed tomography (DESCT) image reveals a part-solid nodule (PSN) or mixed ground-glass opacity (GGO) in the superior lobe of right lung. **b**, **c** The iodine-based material-decomposition images reveal that the iodine concentration (IC) of the nodule is 22.57 μg/cm^3 (L1), the IC of the aorta is 91.33 μg/cm^3 (L2). The normalized IC (NIC) of this lung adenocarcinoma is 0.25 (22.57/91.33). **d** The graph shows the spectral Hounsfield unit (HU) curve of the nodule and that the slope of the spectral attenuation curve (slope λ HU) is 1.74. **e** The molecular pathological result post-surgery reveals the presence of epidermal growth factor (EGFR) mutations

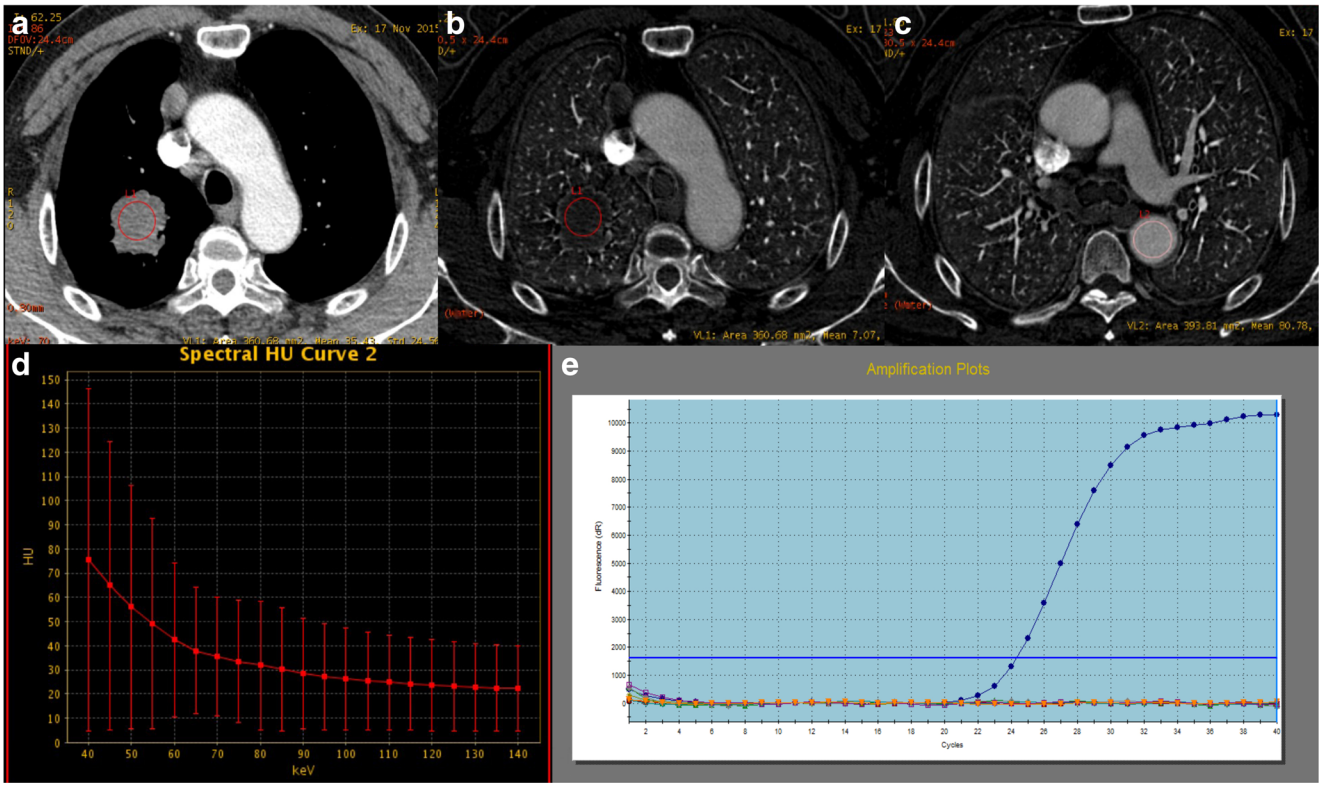

Fig. 3 Images of a 65-year-old male patient with smoking history, diagnosed pulmonary adenocarcinoma. **a** A dual-energy spectral computed tomography (DESCT) image reveals a solid nodule (SN) in the superior lobe of right lung. **b**, **c** The iodine-based material-decomposition images reveal that the iodine concentration (IC) of the nodule is 7.07 μg/cm^3 (L1), the IC of the aorta is 80.78 μg/cm^3 (L2). The normalized IC (NIC) of this lung adenocarcinoma is 0.09 (7.07/80.78). **d** The graph shows the spectral Hounsfield unit (HU) curve of the nodule and that the slope of the spectral attenuation curve (slope λ HU) is 1.33. **e** The molecular pathological result post-surgery reveals no epidermal growth factor (EGFR) mutations (i.e., wild-type)

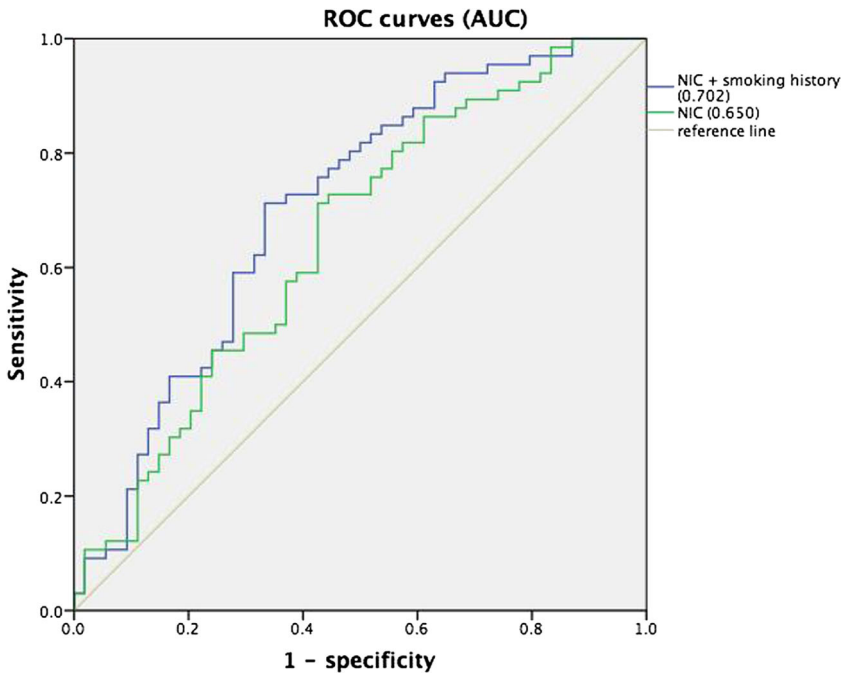

Fig. 4 A receiver operating characteristic (ROC) curve of the normalized iodine concentration (NIC) for the prediction of epidermal growth factor receptor (EGFR) mutations in lung adenocarcinoma (green line); the area under the curve (AUC) is 0.650 (95% confidence interval [CI] 0.551–0.750, $p < 0.005$). The ROC curve for the combined NIC and smoking history for the prediction of EGFR mutation in lung adenocarcinoma (blue line); the AUC is 0.702 (95% CI 0.607–0.798, $p < 0.000$)

significantly higher than those of the EGFR wild-type group ($p = 0.010$), which has not been reported previously. Since iodine is the main component of the CT contrast medium, measuring the iodine concentration using an iodine density image reflects the enhancement of lesions and could have potential for assessing the relative vascularity of small pulmonary nodules [30, 31]. Our results may be attributed to the rich blood supply of lung adenocarcinomas with EGFR mutations. Studies have shown that in addition to cancer genesis and development, EGFR also plays important roles in both physiological and pathological angiogenesis through its effects in endothelial cells and tumor cells by producing angiogenic signals, thereby stimulating angiogenesis through a very complicated biological process [32, 33]. The tumor angiogenesis induced by EGFR may result in an increased blood supply in lung adenocarcinomas with EGFR mutations, and this increase may be embodied by the NIC quantitative parameter.

Unlike previous radio-genomic studies that focused on correlations between conventional CT features and EGFR mutations in lung adenocarcinoma, our study elucidates the possible correlations between DESCT quantitative parameters and EGFR mutations with histologically confirmed pulmonary adenocarcinoma. To the best of our knowledge, our result was the first time to demonstrate that NIC might be a potential quantitative index for predicting EGFR mutations in lung adenocarcinoma. In addition to NIC, the univariate analysis revealed that the slope λ HU value in the EGFR mutation group was also significantly different from that in the EGFR wild-type group ($p = 0.015$). Theoretically, each material has its unique X-ray linear attenuation coefficient, so the curve slope λ HU obtained by DESCT is a relatively accurate quantitative data for material identification [34, 35]. This finding suggests that the slope λ HU might be potentially used to differentiate EGFR status in lung adenocarcinomas. However, the slope λ HU was not a significant factor in our multivariate logistic analysis.

On conventional CT images, GGO is a relatively significant and important texture observed in lung adenocarcinomas compared to other solid tumors. In this study, the PSN or mixed GGO rate in tumors with EGFR mutations was obviously higher than that in EGFR wild-type tumors (18.2% vs. 3.7%), which is consistent with findings from previous studies [8–11]. This phenomenon may be due to the fact that EGFR mutations appear more frequently in lepidic predominant adenocarcinomas [36, 37]. Moreover, the CT number at 70 keV in GGO was quite different from that in solid nodules which due to the extremely low CT number of air. This interference may explain why the CT number at 70 keV was not a significant factor in this study, despite the fact that the CT number can also reflect iodine attenuation in tumors. However, a previous study conducted by Aoki et al found that the NIC was not affected by GGO, unlike the CT number [38]. Additionally, Kawai et al reported that contrast enhancement of GGO can be evaluated using contrast mapping images by DESCT [39]. These studies suggest that iodine quantification, unlike CT number, is hardly affected by GGO component. Therefore, the NIC could be a reliable and accurate imaging biomarker to evaluate the difference in blood volume between tumor subtypes [40].

In this East Asian patient cohort study, 55.1% (66/120) of the cases were identified as EGFR mutations. Besides the ethnicity factor, EGFR mutations were also correlated with specific clinical characteristics, including nonsmoking status and the female sex, which is consistent with the previous studies [6, 7]. Furthermore, multivariate analysis revealed that smoking status was a significant predictive factor in addition to the NIC. Combining these two significant factors (smoking history and the NIC), results demonstrated a moderate predictive value for EGFR mutations identification in pulmonary adenocarcinomas (AUC = 0.702, $p < 0.000$; Fig. 4).

Indeed, our study still had several limitations. First, the data came from a single center and the enrolled sample size was relatively small; however, the homogeneity of the study population with a high EGFR mutation rate enabled identification of significant associations in the absence of a larger population analysis. Second, since the GSI viewer software did not support 3D volume analysis of tumors, the evaluation process was only 1 single slice per tumor, which did not take into account the entire biology features of the lesion. Third, in the patients of the EGFR wild-type group, there were also many different oncogenes present, such as ALK and KRAS, which require further refined study.

In conclusion, this study demonstrated that the NIC from contrast-enhanced DESCT might be a potential predictive quantitative parameter for identification of EGFR mutations in patients with pulmonary adenocarcinoma. The ability to identify this therapeutic target may facilitate personalized precision treatment of patients with this disease.

Funding This study has received funding by the National Natural Science Foundation of China (Grant No. 81601494) and the PUMC Youth Fund/Fundamental Research Funds for the Central Universities (Grant No. 3332016030).

Compliance with ethical standards

Guarantor The scientific guarantor of this publication is Ning Wu.

Conflict of interest The authors of this manuscript declare no relationships with any companies, whose products or services may be related to the subject matter of the article.

Statistics and biometry Ni Li kindly provided statistical advice for this manuscript.

Informed consent Written informed consent was waived by the Institutional Review Board.

Ethical approval Institutional Review Board approval was obtained.

Methodology
- retrospective
- observational
- performed at one institution

References

1. Zhang L, Li M, Wu N, Chen Y (2015) Time trends in epidemiologic characteristics and imaging features of lung adenocarcinoma: a population study of 21,113 cases in China. PLoS One 10:e0136727
2. Auerbach O, Garfinkel L (1991) The changing pattern of lung carcinoma. Cancer 68:1973–1977
3. Travis WD (2009) Reporting lung cancer pathology specimens. Impact of the anticipated 7th edition TNM classification based on recommendations of the IASLC staging committee. Histopathology 54:3–11
4. Zhou C, Wu YL, Chen G et al (2015) Final overall survival results from a randomised, phase III study of erlotinib versus chemotherapy as first-line treatment of EGFR mutation-positive advanced non-small-cell lung cancer (OPTIMAL, CTONG-0802). Ann Oncol 26: 1877–1883
5. Maemondo M, Inoue A, Kobayashi K et al (2010) Gefitinib or chemotherapy for non-small-cell lung cancer with mutated EGFR. N Engl J Med 362:2380–2388
6. Rosell R, Moran T, Queralt C et al (2009) Screening for epidermal growth factor receptor mutations in lung cancer. N Engl J Med 361: 958–967
7. Dearden S, Stevens J, Wu YL, Blowers D (2013) Mutation incidence and coincidence in non small-cell lung cancer: meta-analyses by ethnicity and histology (mutMap). Ann Oncol 24:2371–2376
8. Goo JM, Park CM, Lee HJ (2011) Ground-glass nodules on chest CT as imaging biomarkers in the management of lung adenocarcinoma. AJR Am J Roentgenol 196:533–543
9. Liu Y, Kim J, Qu F et al (2016) CT features associated with epidermal growth factor receptor mutation status in patients with lung adenocarcinoma. Radiology 280:271–280
10. Yang Y, Yang Y, Zhou X et al (2015) EGFR L858R mutation is associated with lung adenocarcinoma patients with dominant ground-glass opacity. Lung Cancer 87:272–277
11. Hong SJ, Kim TJ, Choi YW, Park JS, Chung JH, Lee KW (2016) Radiogenomic correlation in lung adenocarcinoma with epidermal growth factor receptor mutations: imaging features and histological subtypes. Eur Radiol 26:3660–3668
12. Kim TJ, Lee CT, Jheon SH, Park JS, Chung JH (2016) Radiologic characteristics of surgically resected non-small cell lung cancer with ALK rearrangement or EGFR mutations. Ann Thorac Surg 101: 473–480
13. Cheng Z, Shan F, Yang Y, Shi Y, Zhang Z (2017) CT characteristics of non-small cell lung cancer with epidermal growth factor receptor mutation: a systematic review and meta-analysis. BMC Med Imaging 17:5
14. Goo HW, Goo JM (2017) Dual-energy CT: new horizon in medical imaging. Korean J Radiol 18:555–569
15. Johnson TR, Krauss B, Sedlmair M et al (2007) Material differentiation by dual energy CT: initial experience. Eur Radiol 17:1510–1517
16. Simons D, Kachelriess M, Schlemmer HP (2014) Recent developments of dual-energy CT in oncology. Eur Radiol 24:930–939
17. De Cecco CN, Darnell A, Rengo M et al (2012) Dual-energy CT: oncologic applications. AJR Am J Roentgenol 199:S98–S105
18. González-Pérez V, Arana E, Barrios M et al (2016) Differentiation of benign and malignant lung lesions: dual-energy computed tomography findings. Eur J Radiol 85:1765–1772
19. Wang G, Zhang C, Li M, Deng K, Li W (2014) Preliminary application of high-definition computed tomographic gemstone spectral imaging in lung cancer. J Comput Assist Tomogr 38:77–81
20. Sudarski S, Hagelstein C, Weis M, Schoenberg SO, Apfaltrer P (2015) Dual-energy snap-shot perfusion CT in suspect pulmonary nodules and masses and for lung cancer staging. Eur J Radiol 84: 2393–2400
21. Hou WS, Wu HW, Yin Y, Cheng JJ, Zhang Q, Xu JR (2015) Differentiation of lung cancers from inflammatory masses with dual-energy spectral CT imaging. Acad Radiol 22:337–344
22. Otrakji A, Digumarthy SR, Lo Gullo R, Flores EJ, Shepard JA, Kalra MK (2016) Dual-energy CT: spectrum of thoracic abnormalities. Radiographics 36:38–52
23. Chae EJ, Song JW, Seo JB, Krauss B, Jang YM, Song KS (2008) Clinical utility of dual-energy CT in the evaluation of solitary pulmonary nodules: initial experience. Radiology 249:671–681
24. Remy-Jardin M, Faivre JB, Pontana F, Molinari F, Tacelli N, Remy J (2014) Thoracic applications of dual energy. Semin Respir Crit Care Med 35:64–73
25. Ohana M, Jeung MY, Labani A, El Ghannudi S, Roy C (2014) Thoracic dual energy CT: acquisition protocols, current applications and future developments. Diagn Interv Imaging 95:1017–1026
26. Hansell DM, Bankier AA, MacMahon H, McLoud TC, Müller NL, Remy J (2008) Fleischner society: glossary of terms for thoracic imaging. Radiology 246:697–722
27. Godoy MC, Naidich DP (2009) Subsolid pulmonary nodules and the spectrum of peripheral adenocarcinomas of the lung: recommended interim guidelines for assessment and management. Radiology 253:606–622
28. Raad RA, Suh J, Harari S, Naidich DP, Shiau M, Ko JP (2014) Nodule characterization: subsolid nodules. Radiol Clin North Am 52:47–67
29. Truong MT, Ko JP, Rossi SE et al (2014) Update in the evaluation of the solitary pulmonary nodule. Radiographics 34:1658–1679
30. Wang L, Liu B, Wu XW et al (2012) Correlation between CT attenuation value and iodine concentration in vitro: discrepancy between gemstone spectral imaging on single-source dual-energy CT and traditional polychromatic X-ray imaging. J Med Imaging Radiat Oncol 56:379–383
31. Knöss N, Hoffmann B, Krauss B, Heller M, Biederer J (2011) Dual energy computed tomography of lung nodules: differentiation of iodine and calcium in artificial pulmonary nodules in vitro. Eur J Radiol 80:e516–e519
32. Manning BD, Cantley LC (2007) AKT/PKB signaling: navigating downstream. Cell 129:1261–1274
33. Gordan JD, Simon MC (2007) Hypoxia-inducible factors: central regulators of the tumor phenotype. Curr Opin Genet Dev 17:71–77
34. Matsuda I, Akahane M, Sato J et al (2012) Precision of the measurement of CT numbers: comparison of dual-energy CT spectral imaging with fast kVp switching and conventional CT with phantoms. Jpn J Radiol 30:34–39
35. Patino M, Prochowski A, Agrawal MD et al (2016) Material separation using dual-energy CT: current and emerging applications. Radiographics 36:1087–1105
36. Travis WD, Brambilla E, Noguchi M et al (2011) International association for the study of lung cancer/American thoracic society/European respiratory society international multidisciplinary classification of lung adenocarcinoma. J Thorac Oncol 6:244–285

37. Lee HJ, Kim YT, Kang CH et al (2013) Epidermal growth factor receptor mutation in lung adenocarcinomas: relationship with CT characteristics and histologic subtypes. Radiology 268:254–264
38. Aoki M, Takai Y, Narita Y et al (2014) Correlation between tumor size and blood volume in lung tumors: a prospective study on dual-energy gemstone spectral CT imaging. J Radiat Res 55:917–923
39. Kawai T, Shibamoto Y, Hara M, Arakawa T, Nagai K, Ohashi K (2011) Can dual-energy CT evaluate contrast enhancement of ground-glass attenuation? Phantom and preliminary clinical studies. Acad Radiol 18:682–689
40. Ascenti G, Mileto A, Krauss B et al (2013) Distinguishing enhancing from nonenhancing renal masses with dual-source dual-energy CT: iodine quantification versus standard enhancement measurements. Eur Radiol 23:2288–2295